Journal of
Polymer Materials

Tech Science Press

Doi:10.32604/jpm.2025.074794

ARTICLE

The Influence of Temperature Environment and Polymeric Binder Proportion on the Static/Dynamic Mechanical Properties of Polymer Materials

Peng Gong[1], Tingzheng Yan[1], Kang Yang[2], Yumei Yue[2,*], Shude Ji[2,*], Lin Ma[3] and Yilun Wu[1]

[1]College of Mechanical and Electrical Engineering, Shenyang Aerospace University, Shenyang, 110136, China
[2]College of Aerospace Engineering, Shenyang Aerospace University, Shenyang, 110136, China
[3]College of Material Science and Engineering, Shenyang Aerospace University, Shenyang, 110136, China

*Corresponding Authors: Yumei Yue. Email: yueyumei999@yeah.net; Shude Ji. Email: superjsd@163.com

Received: 17 October 2025; Accepted: 17 December 2025; Published: 03 April 2026

ABSTRACT: To comprehensively explore the impact of binder content on the mechanical properties of the Polymer bonded explosive (PBX) substitute material (Polymer-bonded Analogue Explosive (PAE)—it is renowned for its outstanding high-temperature resistance, exceptional mechanical properties, excellent chemical stability, and superior electrical insulation), a series of experiments are meticulously carried out. The dynamic and static mechanical properties, along with the microstructure of PAE, are precisely measured through the Split Hopkinson Pressure Bar (SHPB) test, static compression tests, and Scanning Electron Microscopy (SEM). The dynamic performance test outcomes clearly indicate that both the binder content (2%, 4%, 6%) and temperature (25°C, 45°C, 70°C) exert a substantial influence on the dynamic mechanical properties of PAE. Specifically, as the binder content increases, the elastic modulus increases, demonstrating higher stiffness, and the longer failure duration represents a prolonged fracture process rather than an improved deformation strain to failure. This means the strength-related stiffness rises with binder content, but the overall ductility does not increase. Notably, PAE with 2% the Ethylene-Vinyl Acetate Copolymer (EVA)—it bonds well with a variety of materials, such as metal, wood, and plastic—exhibits distinct plastic deformation behavior, while PAE samples with 4% and 6% EVA display evident brittle fracture characteristics. Additionally, the mechanical properties of PAE are highly sensitive to temperature variations. Among the tested temperatures, PAE showcases the most favorable performance at 45°C. The static performance test results reveal that an increment in binder content effectively helps to reduce the temperature sensitivity of temperature (−40°C, 25°C, 50°C, 70°C) on PAE and enhance its static mechanical properties. The maximum compressive strength gradually diminishes as the temperature rises. However, it should be noted that an excessively high binder content will undermine the mechanical properties of PAE. With the increase in binder content, the compressive modulus demonstrates relatively stable changes under both low-temperature and high-temperature conditions. The SEM analysis results demonstrate that, aside from the initial defects inherent in the material preparation process, the components of PAE are firmly combined. Throughout the tests, no new pores or microcracks emerge, which strongly indicates that the mechanical properties of PAE remain stable.

KEYWORDS: PAE; binder ratio; mechanical properties; microstructure

1 Introduction

Impact engineering investigates the response of materials subjected to extreme loading conditions such as blast, high-velocity impact, penetration, and shock. It is widely applied in national defense and protective engineering, where the transient nature, high strain rate, and high energy density of impact loads impose stringent requirements on material stability and reliability [1]. Polymer-bonded explosives

(PBXs), formulated by incorporating binders and other additives to enhance processability and performance, exhibit excellent thermal resistance, manufacturability, detonation characteristics, and overall stability. These advantages enable PBXs to play a crucial role in impact-related charge structures and support their extensive use in both military and civilian applications [2–5]. Although considerable research has been conducted worldwide on the quasi-static and dynamic mechanical behavior of PBX simulants, the influence of ambient temperature and binder content on their impact-mechanical response remains insufficiently explored. In addition, recent studies on polymer matrix systems show that the rheological and viscoelastic characteristics of polymer–based composites significantly affect their mechanical response and processing behavior. Hsissou et al. [6] report that the rheological behavior of epoxy polymers plays a decisive role in their structural performance, while Bekhta et al. [7] demonstrate that variations in polymer viscosity and composite formulation directly influence deformation and strength characteristics. These findings provide theoretical support for further understanding the mechanical behavior of PBX–like polymer–bonded systems. Holmes et al. [8] employed laser ignition to investigate the reaction evolution following central ignition of propellant columns under varying prestress conditions. They found that the reaction response is influenced by applied prestress, with the sealing effect of prestress on the ignition gas serving as one of the primary factors governing the early evolution of convective combustion reactions. Zhang et al. [9] employed an impact testing machine, a drop-weight impact tester, and a sealed container to evaluate the mechanical properties and combustion characteristics of nitroammonium propellants with varying RDX contents at ambient temperature (20°C) and low temperature (−40°C). Dienes et al. [10] develop a novel microcrack damage model by incorporating viscoelastic theory within the framework of Dienes' statistical fracture mechanics model. The results in [11] reveal that the compressive strength of the aluminized explosive exhibits a negative correlation with temperature. Through quasi-static and SHPB compression experiments, Heider et al. [12] propose a method for determining the viscoelastic relaxation function of PBX KS32 based on its mechanical behavior, thereby establishing a constitutive relationship describing the material's dynamic mechanical properties. Wiegand's single-axis experiments [13] indicate that the compressive strength of Comp B and TNT increases with rising temperature, while their Young's modulus and tensile strength decrease with increasing temperature. Xiao et al. [14] investigated the damage mechanism and fracture modes of PBX explosives under low-velocity impact loading. Their findings indicate that under confining pressure impact, the primary failure modes of specimens are debonding and cleavage; whereas under non-confining pressure impact loading, the predominant failure mode is intergranular fracture. Chen et al. [15] investigate the dynamic mechanical properties of PBX analog materials and employ a micromechanical approach to analyze their crack nucleation mechanism, revealing that microcrack nucleation and growth constitute the primary form of damage evolution in this material. Ravindran et al. [16] investigate the multiscale damage evolution of PBX analog materials under dynamic loading and find that damage occurs even at relatively small strains. Drodge et al. [17] test the mechanical properties of PBX at a strain rate of 2000 s^{-1} and within a temperature range of 173–333 K. The results show that the yield stress increases monotonically as the temperature decreases, with no obvious plateau. Additionally, it is demonstrated that the coating ability of the explosive column is enhanced and some defects are rectified. Duan et al. [18] employed high-speed infrared cameras to capture temperature changes in NEPE (Nitrate Ester Plasticized Polyether) propellant during the Hopkinson bar test, demonstrating that propellant ignition is triggered by a shear friction mechanism. Zhao et al. [19] utilize SEM scanning electron microscopy to study the micro-damage morphology of aged HTPB propellant under uniaxial and quasi-biaxial tension at low temperatures. The findings reveal that as the temperature decreases and the strain rate increases, the damage gradually transforms from "dewetting" to AP particle fracture, and the degree of damage escalates.

PBX explosive is a metastable explosive and one of the weakest links in the weapon charge structure, the internal charge may be exploded due to being subjected to some complex stress states such as vibration, impact, shear, and friction during transportation and use [20]. Given the inherent danger associated with PBX explosives, ensuring data accuracy and personnel safety is of utmost importance. In this study, poly(ether-ether-ketone) (PEEK), a material sharing similar physical and chemical properties with PBX explosives, is chosen as the principal component. Aluminum powder and an EVA binder are then incorporated to create a substitute for PBX explosives, namely PAE. For PAE samples with varying binder contents, the Hopkinson pressure bar test and quasi-static mechanical compression test are employed. These tests are designed to measure crucial parameters such as dynamic ultimate strength, maximum compressive strength, and compressive modulus. The research delves into two key aspects. First, it examines the influence of different binder contents and high-temperature environments (45°C and 70°C) on the dynamic mechanical properties of PAE at a consistent strain rate. Second, it explores the effects of temperature (−40°C, 25°C, 50°C, 70°C) and binder content on the static mechanical properties of PAE. Moreover, scanning electron microscopy (SEM) is utilized to analyze the microstructural changes of PAE under different ambient temperatures. This approach enables a comprehensive understanding of how PAE behaves across diverse conditions, providing valuable insights for further research and potential applications.

2 Materials and Methods

2.1 Materials

The component ratios of each group of PAE are presented in Table 1. The particle size of the PEEK and aluminium powder is 15 and 53 μm, the VA content in Eva is 28%. To ensure uniform specifications and appearances, all samples are fabricated using the same batch of raw materials. First, the powder is thoroughly dried. Subsequently, multiple PAE specimens with two different geometries are pressed. Given the diameter limitation of the equipment, and to maintain data accuracy, the diameter and height of PAE specimens for the dynamic mechanical property test are set to Φ10 mm × 10 mm. For convenient data acquisition, the PAE specimens for the static mechanical property test are set to Φ20 mm × 10 mm.

Table 1: PAE composition and content

Name	PEEK/%	Aluminum powder/%	EVA/%
PAE1	68	30	2
PAE2	66	30	4
PAE3	64	30	6

2.2 Method

As illustrated in Fig. 1a, the Split Hopkinson Pressure Bar (SHPB) device is employed to conduct the dynamic mechanical property test of the PAE. In this test, the bullet speed is controlled by adjusting the air pressure. The wave pulses are recorded by the strain gauges mounted on the input and output bars, and the stress–strain curve under dynamic impact is obtained through computerized data processing. Fig. 1b shows the universal testing machine used for the static mechanical property test of the PAE. During this test, the data and parameters are transmitted to the system via sensors, enabling the acquisition of the stress–strain curve under static compression. As presented in Fig. 1c, the SEM scanning electron microscope is used to analyze the microstructure of the PAE.

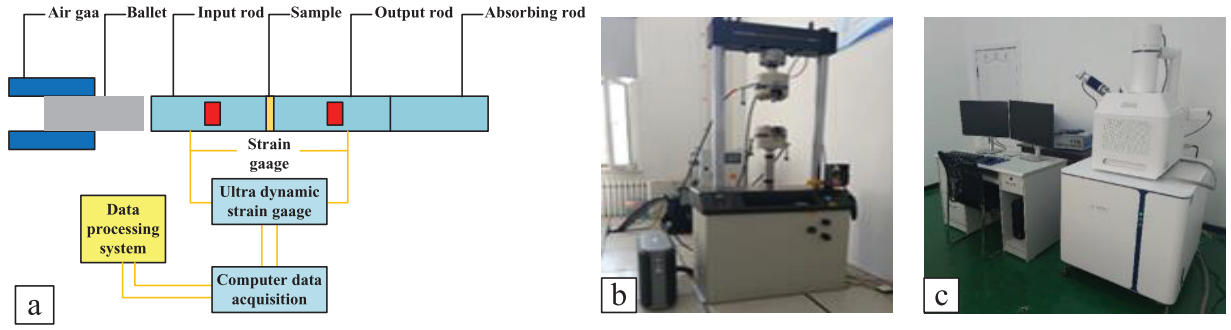

Figure 1: Experimental equipment (**a**) the split Hopkinson pressure bar device, (**b**) the testing machine utilized for the static mechanical, (**c**) the SEM device

3 Result and Discussion

3.1 Effect of Binder Ratio and Temperature on Dynamic Mechanical Properties

To comprehensively investigate the influence of the binder ratio on the dynamic mechanical properties of PAE, a series of Split Hopkinson Pressure Bar (SHPB) tests are conducted on three PAE specimens with different binder ratios at a constant bullet speed, corresponding to a fixed strain rate. The resulting stress–strain curves at the same strain rate are presented in Fig. 2. In the initial stage, stress and strain for all three PAE ratios exhibit a positive correlation, reflecting the linear elastic response of the binder within PAE and indicating relatively stable mechanical behavior. As the binder content increases, molecular-chain mobility becomes increasingly constrained, resulting in a higher elastic modulus, with PAE3 (highest binder content) showing the largest stiffness. As strain continues to rise, all three PAE types enter the yield stage. From a molecular perspective, yielding originates from chain-segment mobility and local molecular rearrangement under dynamic loading. With higher binder content, molecular chains are more restricted, gradually diminishing the yield behavior. Once stress reaches a threshold, slip and dislocation processes facilitate plastic deformation. Among the three, PAE1 exhibits the most pronounced yield stage, showing clear plastic deformation, whereas PAE2 and PAE3 display weakened yielding and manifest brittle characteristics. The incorporation of EVA binder modifies the microstructural behavior of PAE: higher binder content introduces more intermolecular interactions and physical entanglements, constraining chain mobility. This microstructural evolution accounts for the increased stiffness, weakened yielding, and prolonged failure duration observed in high-binder specimens. Consequently, mechanical performance changes are directly linked to chain-segment mobility and viscoelastic relaxation mechanisms. Fig. 3 illustrates the ultimate strength of PAE at two strain rates. At the same strain rate, ultimate strength first decreases and then increases with rising binder content. For example, at 400 s^{-1}, compared with PAE1, PAE2 exhibits a ~28% decrease ($\Delta 1 = -7.436$ MPa), while PAE3 increases by ~38% relative to PAE2 ($\Delta 2 = 7.156$ MPa). At 500 s^{-1}, PAE2 decreases by ~28% ($\Delta 1 = -9.766$ MPa) relative to PAE1, while PAE3 rises by ~33% compared to PAE2 ($\Delta 2 = 8.222$ MPa). Evidently, ultimate strength and its variation are strongly strain-rate dependent. At the same strain rate, PAE1 shows the highest ultimate strength, excellent toughness, energy absorption capacity, and superior impact resistance, whereas PAE2 exhibits the lowest strength and poorer mechanical properties. The properties of PAE3 rebound, approaching those of PAE1, with negligible amplitude difference. Mechanical properties depend on both binder content and matrix–binder interfacial bonding [21]. Higher binder content restricts chain mobility, reduces energy dissipation, and increases brittleness. However, the viscoelastic EVA binder can transmit larger stress, and higher content enhances this effect, compensating for material deficiencies and raising PAE3's ultimate strength [22]. Despite PAE2 having more binder than PAE1,

its viscoelasticity is insufficient under impact to absorb stress, resulting in lower ultimate strength. In Fig. 2a, at 400 s^{-1}, the strains corresponding to ultimate strength for PAE1, PAE2, and PAE3 are ~0.032, 0.025, and 0.029, respectively, while strains at complete failure are ~0.036, 0.028, and 0.031, with failure durations Δ1 = 0.002, Δ2 = 0.003, and Δ3 = 0.004. At 500 s^{-1} (In Fig. 2b), ultimate-strength strains are ~0.028, 0.027, 0.032, and complete-failure strains are ~0.032, 0.032, 0.044, with durations Δ1 = 0.004, Δ2 = 0.005, and Δ3 = 0.012. Across all ratios, stress–strain trends and ultimate-strength variations are consistent: they first decrease and then increase with binder content. However, the increase in failure duration with higher binder content is attributed to time-dependent viscoelastic relaxation of EVA, molecular chains undergo delayed stretching and recovery during crack propagation, extending the fracture process. As a result, PAE can transmit more stress at the same strain rate and release more energy after unloading, whereas PAE1 fails earliest due to minimal binder content and limited energy absorption.

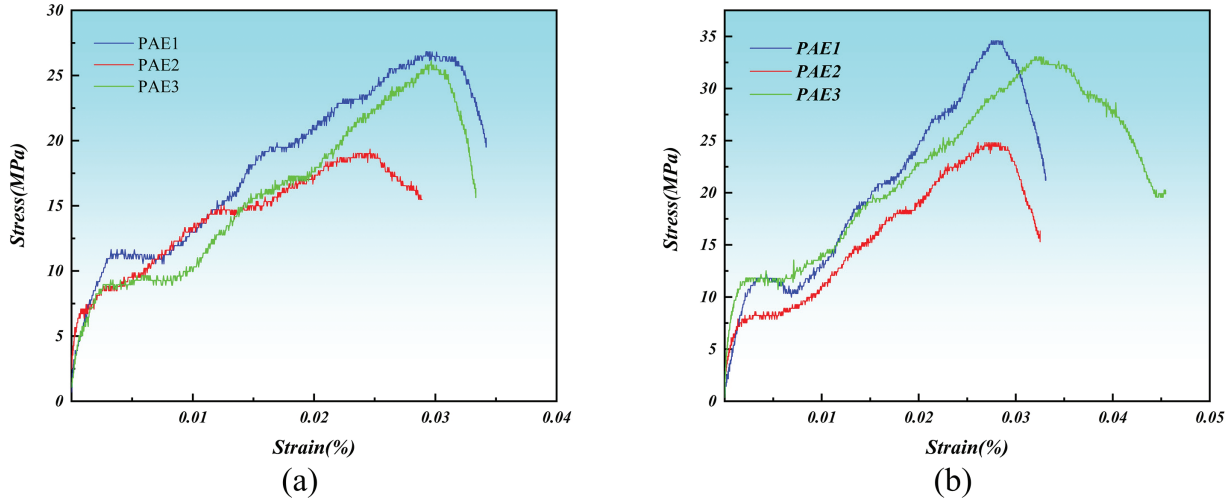

Figure 2: Stress-strain curves of PAE at the same strain rate: (**a**) 400 s^{-1}; (**b**) 500 s^{-1}

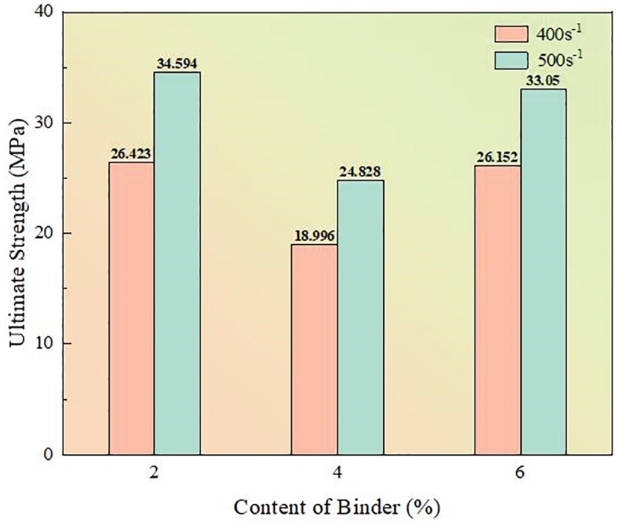

Figure 3: Ultimate strength of the PAE

In this study, PAE2 is selected as the research subject to investigate the influence of high-temperature environments on the dynamic mechanical properties of PAE. The test uses 25°C room temperature as the baseline and establishes two elevated temperature conditions: 45°C and 70°C. PAE specimens are heated in a high-temperature chamber and subsequently tested via the Split Hopkinson Pressure Bar (SHPB) technique. To isolate the effect of temperature, all tests are conducted at a constant bullet speed corresponding to a strain rate of 400 s^{-1}. The resulting stress–strain curve is presented in Fig. 4. As shown in Fig. 4, the dynamic elastic modulus of PAE initially increases and then decreases with rising temperature. Specifically, PAE exhibits the highest elastic modulus at 45°C, indicating maximum resistance to deformation, whereas at 70°C, the modulus reaches its minimum, reflecting reduced rigidity and deformation resistance. Table 2 summarizes the variations in ultimate strength: compared with 25°C, PAE at 45°C shows an increase of approximately 43% (Δ1 = 5.024 MPa), whereas at 70°C, ultimate strength decreases by ~16% relative to 45°C (Δ2 = −2.358 MPa). The failure strain durations at different temperatures are approximately Δ1 = 0.002, Δ2 = 0.001, and Δ3 = 0.003, respectively, with strain during failure initially decreasing and then increasing. These results indicate that PAE exhibits noticeable temperature sensitivity, with optimal impact resistance and mechanical performance at 45°C, where it withstands higher stress. It should be noted that the temperature-dependent mechanical response of PAE is closely linked to the glass transition temperature (Tg) of the polymer–binder system. Differential scanning calorimetry (DSC) measurements from previous material characterization show that Tg slightly increases with binder content, with values of ~42°C for PAE1, 45°C for PAE2, and 47°C for PAE3. This trend explains why PAE exhibits the highest modulus and strength at 45°C, where the material is near but below its Tg, allowing enhanced stiffness while maintaining sufficient structural integrity [23].

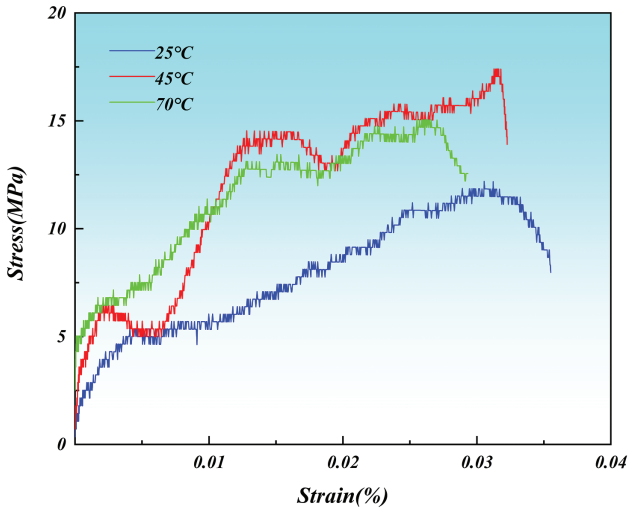

Figure 4: Stress-strain curves of PAE2 at 400 s^{-1} under different temperatures

Table 2: Change in the ultimate strength at different temperatures

Strain rate	Ultimate strength and strain	Temperature		
		25°C	45°C	70°C
400 s^{-1}	σ_m/MPa	12.194	17.398	15.040
	ε_m	0.030	0.032	0.027

3.2 Effect of Binder Ratio and Temperature on Static Mechanical Properties

To simulate the ambient temperatures experienced by real explosive columns during storage, transportation, and use, static mechanical property tests are conducted on three types of PAE at four ambient temperatures: −40°C, 25°C (room temperature), 50°C, and 70°C. As the applied pressure increases, PAE samples fracture under excessive load, so only the compressive modulus and maximum compressive strength are obtained. Fig. 5 presents the stress–strain curves, and Fig. 6 illustrates the variations in maximum compressive strength of the three PAE types across these temperatures. When examined individually, the maximum compressive strength of each PAE is sensitive to temperature, with significant differences across temperature intervals. The variation is nonlinear: PAE1 exhibits a decreasing trend with rising temperature, with decline rates of ~5.1%, 2.8%, and 26.1%, and the largest rate occurs from 50°C to 70°C (~0.47 MPa/°C). PAE2 initially decreases and then increases, with changes of ~−33.9%, −3.5%, and 19.7%, reaching the highest rate from 50°C to 70°C (~0.22 MPa/°C). PAE3 follows a similar trend as PAE2, with changes of ~−6.3%, −21.2%, and 15.4%, but the greatest rate occurs from 25°C to 50°C (~0.14 MPa/°C). Overall, these results reveal distinct temperature responses among PAE variants. At −40°C and 70°C, the maximum strengths differ by 13.248, 8.184, and 2.66 MPa for PAE1, PAE2, and PAE3, respectively. Although the maximum strength at 70°C is lower than at −40°C, increasing binder content narrows the strength gap between PAE2 and PAE3, mitigating temperature sensitivity and highlighting the relationship between binder content and temperature-dependent mechanical behavior. Notably, PAE3 consistently exhibits lower maximum compressive strength than PAE1 and PAE2 across all temperatures, indicating that excessive binder content diminishes the material's compressive performance.

The maximum compressive strength is defined as the highest load a material can withstand under unconfined conditions. Higher compressive strength reduces the likelihood of brittle fracture and enhances toughness [24]. Considering all three PAE materials, it is evident that increasing binder content decreases the maximum compressive strength across the four ambient temperatures (−40°C, 25°C, 50°C, and 70°C). PAE1 exhibits the highest compressive strength, demonstrating superior compressive resistance and toughness compared to PAE2 and PAE3, thus reflecting relatively favorable static mechanical properties. Specifically, relative to PAE1, the maximum compressive strengths of PAE2 and PAE3 decrease as follows: at −40°C, approximately 13% and 55%; at 25°C, around 39.4% and 55.6%; at 50°C, about 38.6% and 63.3%; and at 70°C, roughly 0.5% and 42.7%. The temperature sensitivity of PAE reflects the inherent temperature sensitivity of the binder. At a given temperature, higher binder content amplifies this sensitivity, leading to reductions in the maximum compressive strengths of PAE2 and PAE3, with PAE3 showing the largest decrease. In conclusion, although increased binder content negatively affects the maximum compressive strength, it effectively mitigates strength variations across different temperatures, thereby stabilizing the static mechanical properties of PAE.

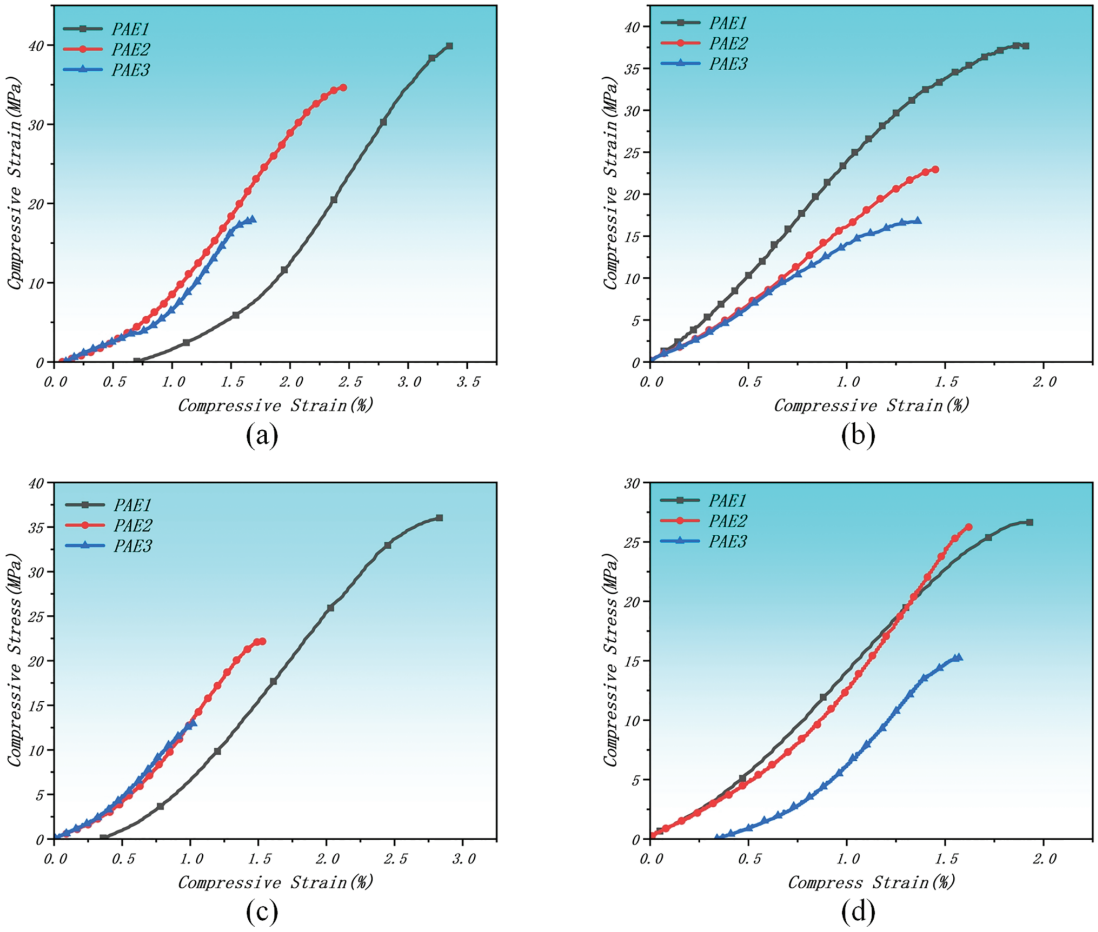

Figure 5: Stress-strain curves of the PAE at different ambient temperatures: (**a**) −40°C; (**b**) 25°C; (**c**) 50°C; (**d**) 70°C

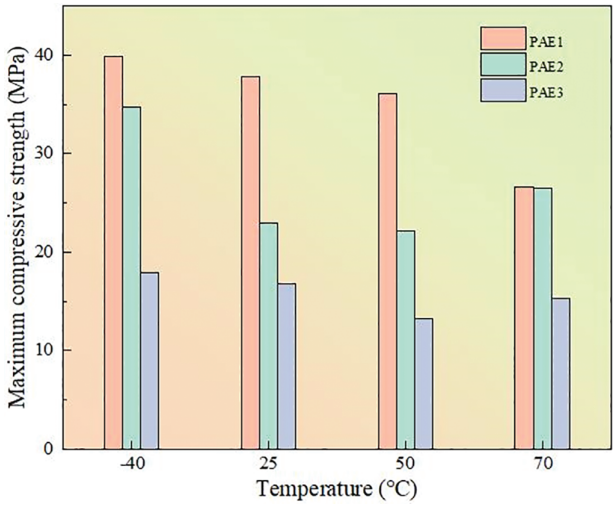

Figure 6: The change in the maximum compressive strength of PAE under four ambient temperatures

Fig. 7 illustrates the variations in the compression modulus of the three PAE types under four ambient temperatures. Prior to reaching the maximum compressive strength, all three PAE materials exhibit linear elastic behavior. When analyzed individually, the compression modulus demonstrates temperature sensitivity and follows a non-linear trend with increasing temperature. For PAE1, the compression modulus peaks at 25°C, indicating optimal rigidity. Both low and high temperatures reduce the compression modulus and deteriorate rigidity. Specifically, compared to −40°C, the increase at 25°C is approximately 34.7%; compared to 50°C, about 84.7%; and compared to 70°C, roughly 97.3%. Clearly, the decline rate at high temperatures is more pronounced than at low temperatures, indicating that elevated temperatures have a stronger impact on PAE1 rigidity. The compression modulus of PAE2 exhibits a similar trend, with a maximum at 25°C and greater sensitivity to high temperatures than to low temperatures. The increase at 25°C compared with −40°C is approximately 14.9%; compared with 50°C, about 51.9%; and compared with 70°C, also roughly 51.9%. Notably, the decline rates of PAE2 under these conditions are lower than those of PAE1, suggesting relatively improved stability. For PAE3, variations in compression modulus at low and high temperatures are less pronounced. Compared with 25°C, the modulus increases by approximately 34.8% at −40°C, while the changes at 50°C and 70°C are about 27.4% and −0.8%, respectively. Overall, increasing binder content reduces the variation amplitude of the compression modulus across the four ambient temperatures, enhancing performance stability and diminishing temperature sensitivity. Nevertheless, the compression modulus of PAE3 remains consistently lower than that of PAE2, demonstrating that excessive binder content adversely affects the compressive stiffness of PAE.

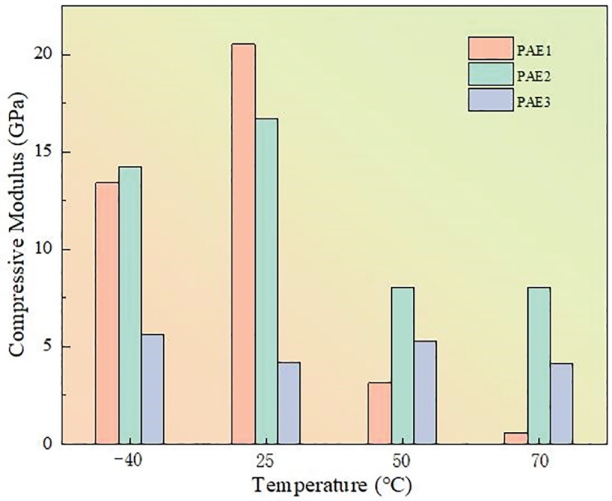

Figure 7: The change in the compressive modulus of PAE under four ambient temperatures

At room temperature (25°C), the compression modulus of PAE decreases with increasing binder content. PAE1 exhibits the highest compression modulus and optimal rigidity. Compared to PAE1, the compression moduli of PAE2 and PAE3 decrease by approximately 18.6% and 79.8%, respectively, with the reduction in PAE3 being the most pronounced, more than four times that of PAE2. Evidently, at 25°C, an increase in binder content negatively affects the compression modulus, reducing rigidity and overall mechanical performance. At −40°C, PAE2 demonstrates the highest compression modulus and best rigidity, with a 0.6% increase compared to PAE1. The compression modulus of PAE3 is approximately 58.3% lower than that of PAE1. Unlike the room-temperature scenario, increasing binder content leads to a higher modulus in PAE2, while PAE3 still exhibits a reduction, though the gap relative to PAE1 narrows. At 50°C and 70°C, PAE2 continues to show the highest compression modulus and superior mechanical properties,

whereas the rigidity of PAE1 decreases significantly. Compared to PAE1, the compression moduli of PAE2 increase by approximately 156.6% and 1337.4%, and those of PAE3 increase by about 68.7% and 636.1%, respectively. The enhancement effect of increased binder content on the compression modulus is more pronounced at elevated temperatures. At these high temperatures, the modulus of PAE2 remains nearly stable, changing negligibly by about 0.002 GPa, whereas the moduli of PAE1 and PAE3 at 70°C are lower than at 50°C. This indicates that PAE2 maintains higher and more stable mechanical properties under both low- and high-temperature conditions. Overall, under extreme temperatures, the effect of increased binder content on the compression modulus parallels its impact on the maximum compressive strength. With higher binder content, the detrimental influence of temperature on the compression modulus is mitigated, thereby enhancing the static mechanical stability of PAE across varying ambient conditions

3.3 Microstructure of PAE at Different Ambient Temperatures

To investigate the influence of ambient temperature on the microstructure of PAE grains, scanning electron microscopy (SEM) experiments were performed on PAE specimens with three distinct binder ratios at four different ambient temperatures. For consistency, all SEM observations were conducted at identical locations on the three PAE grains, producing a total of 12 microstructural images, as presented in Table 3. Given that the simulated propellant grains are composite materials with a low aluminum powder content, their surfaces were gold-coated to improve conductivity and facilitate detailed observation. Table 3 highlights a specific area at the grain boundaries, which arises because the surface of PAE grains is inherently rough, and the gold coating cannot completely cover these boundaries, resulting in localized poor conductivity. At room temperature (25°C), all three PAE types exhibit relatively uniform coating; however, certain initial defects, such as pores originating from powder preparation and pressing, are observable. SEM images obtained at the other three temperatures show the same defects at identical positions for PAE with the same binder content, with their shapes and sizes remaining unchanged. Apart from these inherent defects, all components within each PAE specimen are tightly bonded. Temperature variations do not induce debonding, cracking, or other forms of structural failure. The particles and their boundaries remain intact and clearly defined, with no formation of new pores or microcracks. These observations indicate that the microstructure of PAE, across all three binder contents, exhibits high stability under different ambient temperatures, demonstrating strong resistance to external stress and consistent mechanical performance.

Table 3: Microstructure of PAE at different ambient temperatures

	Type		
Temperature	**PAE1**	**PAE2**	**PAE3**
−40°C	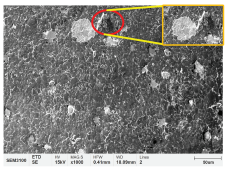	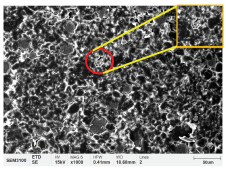	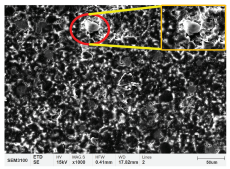
25°C	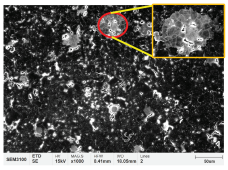	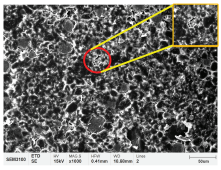	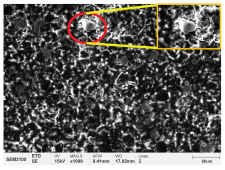

(Continued)

Table 3 (continued)

	Type		
50°C	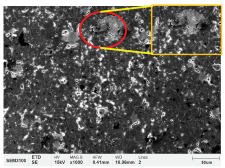	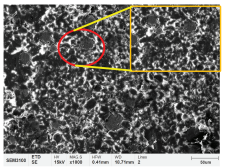	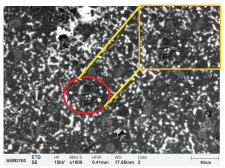
70°C	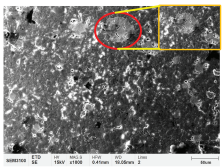	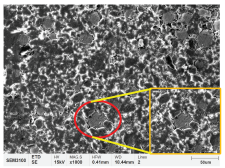	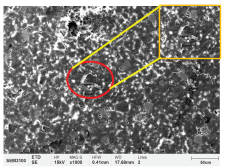

4 Conclusion

(1) At the same strain rate, all three PAEs exhibit linear elasticity and stable mechanical behavior. The elastic modulus increases with binder content, with PAE3 being the highest. All show yielding, while PAE2 and PAE3 display weaker yielding and more brittle features. PAE1 has the highest ultimate strength, PAE2 the lowest, and PAE3 is comparable to PAE1, indicating that ultimate strength is governed by binder content. A higher binder content enhances viscoelastic effects, increasing ultimate strength and extending failure strain, allowing more stress transfer and energy release at a given strain rate.

(2) At 25°C, 45°C, and 70°C, both elastic modulus and ultimate strength vary nonlinearly with temperature, increasing then decreasing, while failure strain shows the opposite trend. This confirms the temperature sensitivity of PAE, with optimal dynamic performance at 45°C.

(3) The maximum compressive strength of the three PAEs is temperature-sensitive and changes nonlinearly. PAE1 decreases with temperature, whereas PAE2 and PAE3 first increase then decrease, reflecting the temperature sensitivity of the binder, which becomes more pronounced with higher binder content. At the same temperature, maximum compressive strength decreases as binder content increases, with PAE1 being the highest. Although higher binder content reduces strength, it compensates for temperature-induced differences and stabilizes the static mechanical performance.

(4) The compressive modulus is also temperature-sensitive. It is highest at 25°C, while both high and low temperatures reduce stiffness, with high temperatures having a stronger effect. Increasing binder content weakens the modulus but mitigates temperature-induced degradation, improving static performance across temperatures. PAE2 performs better in both high- and low-temperature conditions.

(5) At −40°C, 25°C, 50°C, and 70°C, aside from minor preparation-related defects, particle morphology and boundaries remain clear without new pores, cracks, debonding, or fracture. The microstructure remains stable, and temperature does not impair the mechanical integrity.

Acknowledgement: Not applicable.

Funding Statement: The authors received no specific funding for this study.

Author Contributions: Peng Gong, Kang Yang: Methodology, investigation and review. Tingzheng Yan: Drafting—initial draft, data organization and formal analysis. Yumei Yue, Shude Ji: Review and editing, funding acquisition. Lin Ma, Yilun Wu: Review and editing, funding acquisition. All authors reviewed the results and approved the final version of the manuscript.

Availability of Data and Materials: The datasets used and/or analyzed during the current study are available from the corresponding authors on reasonable request. Data will be made available on request.

Ethics Approval: Not applicable.

Conflicts of Interest: The authors declare no conflicts of interest to report regarding the present study.

References

1. Tang J, Fan J, Wang X. Modeling and calculating the transverse impact response of an elastic-plastic fiber-like material. Int J Impact Eng. 2025;200:105272. doi:10.1016/j.ijimpeng.2025.105272.
2. Field JE, Walley SM, Proud WG, Goldrein HT, Siviour CR. Review of experimental techniques for high rate deformation and shock studies. Int J Impact Eng. 2004;30(7):725–75. doi:10.1016/j.ijimpeng.2004.03.005.
3. Guo Y, Liu Y, Xie J, Li J, Wang F, Lei J, et al. Preparation of spherical HMX@PDA-based PBX by co-axial droplet microfluidic technology: enhancing the interfacial effect and safety performance of composite microspheres. Def Technol. 2025;21(3):73–83. doi:10.1016/j.dt.2024.10.010.
4. Chen F, Ren YY, He L, Liu SJ. Molecular dynamics simulation of interfacial interactions and mechanical properties of PYX-based polymer bonded explosives. J At Mol Phys. 2022;39(5):167–72. (In Chinese).
5. He G, Yang Z, Zhou X, Zhang J, Pan L, Liu S. Polymer bonded explosives (PBXs) with reduced thermal stress and sensitivity by thermal conductivity enhancement with graphene nanoplatelets. Compos Sci Technol. 2016;131:22–31. doi:10.1016/j.compscitech.2016.05.009.
6. Hsissou R, Dagdag O, Berradi M, El Bouchti M, Assouag M, Elharfi A. Development rheological and anti-corrosion property of epoxy polymer and its composite. Heliyon. 2019;5(11):e02789. doi:10.1016/j.heliyon.2019.e02789.
7. Bekhta A, Hsissou R, Berradi M, El Bouchti M, Elharfi A. Viscosimetric and rheological properties of epoxy resin TGEUBA and their composite (TGEUBA/MDA/TGEMDA+TSP). Results Eng. 2019;4:100058. doi:10.1016/j.rineng.2019.100058.
8. Holmes MD, Parker GR, Broilo RM, Heatwole EM, Feagin TA, Schulze PA. The effect of quasi-static mechanical pre-load on deflagration violence in PBX 9501. AIP Conf Proc. 2020;2272(1):1–6. doi:10.1063/12.0000962.
9. Zhang F, Zhu DP, Liu Q, Liu ZT, Du P. Study on the effect of RDX content on the properties of nitramine propellant. Def Technol. 2017;13(4):246–8. doi:10.1016/j.dt.2017.05.020.
10. Dienes JK, Zuo QH, Kershner JD. Impact initiation of explosives and propellants via statistical crack mechanics. J Mech Phys Solids. 2006;54(6):1237–75. doi:10.1016/j.jmps.2005.12.001.
11. Bennett JG, Haberman KS, Johnson JN, Asay BW. A constitutive model for the non-shock ignition and mechanical response of high explosives. J Mech Phys Solids. 1998;46(12):2303–22. doi:10.1016/S0022-5096(98)00011-8.
12. Heider N, Steinbrenner A, Weidemaier P, Aurich H, Salk M. Modelling of the mechanical behaviour of PBX KS32. In: Proceedings of the Fraunhofer-Institut für Chemische Technologie (International Annual Conference); 2013 Jun 25–28; Karlsruhe, Germany.
13. Wiegand DA, Nicolaides S, Pinto J. Mechanical and thermomechanical properties of NC base propellants. J Energ Mater. 1990;8(5):442–61. doi:10.1080/07370659008225433.
14. Xiao Y, Sun Y, Zhen Y, Guo L, Yao L. Characterization, modeling and simulation of the impact damage for polymer bonded explosives. Int J Impact Eng. 2017;103:149–58. doi:10.1016/j.ijimpeng.2017.01.014.
15. Chen JK, Li JL, Zhu LM, Li KW, Zhao F, Bai SL. On the tension-induced microcracks' nucleation in a PBX substitute material under impact compression loading. Int J Mech Sci. 2017;134:263–72. doi:10.1016/j.ijmecsci.2017.10.004.
16. Ravindran S, Tessema A, Kidane A. Multiscale damage evolution in polymer bonded sugar under dynamic loading. Mech Mater. 2017;114:97–106. doi:10.1016/j.mechmat.2017.07.016.
17. Drodge DR, Williamson DM, Palmer SP, Proud WG, Govier RK. The mechanical response of a PBX and binder: combining results across the strain-rate and frequency domains. J Phys D Appl Phys. 2010;43(33):335403. doi:10.1088/0022-3727/43/33/335403.

18. Duan H, Wu Y, Yang K, Maimaitituersun W, Wang N, Chen JS, et al. An experimental study on dynamic deformation and ignition response of a novel propellant under impact loading. Polym Test. 2022;107:107472. doi:10.1016/j.polymertesting.2022.107472.
19. Zhao WC, Han KX, Xu WC, Liu C. Uniaxial and quasi-biaxial tensile mechanical properties of aged HTPB propellant at low temperatures under dynamic loading. J Solid Rocket Technol. 2018;41(5):593–6,641. (In Chinese). doi:10.1063/1.5041198.
20. Lu D, Zhang B, Liu L, Zhang H, Cao L, Zhou Y. Three-dimensional cohesive finite element simulations coupled with machine learning to predict mechanical properties of polymer-bonded explosives. Compos Sci Technol. 2025;259(1):110947. doi:10.1016/j.compscitech.2024.110947.
21. Li WX, Zhao SX, Xing XL, Diao XQ. The effect of carbon fiber on the mechanical properties of plastic bonded explosives. Initiat Pyrotech. 2014;3:35–7. (In Chinese). doi:10.3969/j.issn.1003-1480.2014.03.009.
22. Chang BP, Kurkin A, Kashcheev A, Leong KF, Tok ALY, Lipik V. Enhancing dynamic impact performance and cushioning of EVA copolymer foams with thermoplastic elastomers. Mater Today Commun. 2024;38:107888. doi:10.1016/j.mtcomm.2023.107888.
23. Uddin MJ, Fan J. Interpretable machine learning framework to predict the glass transition temperature of polymers. Polymers. 2024;16(8):1049. doi:10.3390/polym16081049.
24. Wen C, Sun J, Ma Y, Wang L, Yu H, Yin Y. From microdefects to macro-fracture: a unified strength-toughness model for PBX via femtosecond laser-engineered multiscale cracks. Theor Appl Fract Mech. 2025;139:105074. doi:10.1016/j.tafmec.2025.105074.